

Huge linear magnetoresistance due to open orbits in γ -PtBi₂

Beilun Wu,¹ Víctor Barrena,¹ Hermann Suderow,^{1,2} and Isabel Guillamón^{*1,2}

¹Laboratorio de Bajas Temperaturas y Altos Campos Magnéticos,
Departamento de Física de la Materia Condensada,
Instituto Nicolás Cabrera and Condensed Matter Physics Center (IFIMAC),
Universidad Autónoma de Madrid, E-28049 Madrid, Spain

²Unidad Asociada de Bajas Temperaturas y Altos Campos Magnéticos,
UAM, CSIC, Cantoblanco, E-28049 Madrid, Spain

Some single-crystalline materials present an electrical resistivity which decreases between room temperature and low temperatures at zero magnetic field as in a good metal and switches to a nearly semiconductinglike behavior at low temperatures with the application of a magnetic field. Often, this is accompanied by a huge and nonsaturating linear magnetoresistance which remains difficult to explain. Here, we present a systematic study of the magnetoresistance in single-crystal γ -PtBi₂. We observe that the angle between the magnetic field and the crystalline c axis fundamentally changes the magnetoresistance, going from a saturating to a non-saturating magnetic-field dependence. In between, there is one specific angle where the magnetoresistance is perfectly linear with the magnetic field. We show that the linear dependence of the nonsaturating magnetoresistance is due to the formation of open orbits in the Fermi surface of γ -PtBi₂.

Magnetoresistance (MR) is the modification of the electrical resistance by a magnetic field. MR is a ubiquitous phenomenon in metals and semiconductors, although it is not expected to occur just considering free electrons without interactions. The electrical resistivity ρ occurs due to scattering of electrons on a timescale τ , and the main consequence of applying a magnetic field is spiraling the electron orbits with an angular velocity $\omega_c = \frac{eB}{m^*}$ (with e as the electron charge and m^* as the electronic effective mass). When considering nearly free electrons, the simplest magnetic field dependence found for the magnetoresistance is quadratic $\rho(B) \propto B^2$, obeying Onsager's reciprocity condition $\rho(B) = \rho(-B)$. Furthermore, the MR saturates in the high field limit ($\omega_c\tau \gg 1$) unless electron and hole numbers are close to compensate with each other, in which case it continues growing as $\rho(B) \propto B^2$. In metals with no or weak electronic correlations, a small quadratic MR saturating at high fields is indeed often observed¹⁻³, with a few exceptions such as the semimetal Bi and other electron-hole compensated metals⁴⁻⁷. More intriguing and difficult to explain is the observation of a huge and nonsaturating linear magnetoresistance, which has been recently discussed in a number of materials. The magnetoresistance is also influenced by contributions from open orbits, which play sometimes a role, often leading to a sizable enhancement, which was however not considered as sufficient to explain huge magnetoresistances¹⁻³. Here, we show that the direction of the magnetic field produces an unanticipated huge enhancement of the linear magnetoresistance exactly when the contribution of open orbits to the magnetoresistance is maximal.

There are a number of metallic or semimetallic compounds showing large and sometimes linear magnetoresistances⁷⁻²². The semimetal γ -PtBi₂ stands out among these compounds because of the extreme values of the magnetoresistance²³. γ -PtBi₂ has a layered structure with trigonal symmetry (space group

$P31m$, No.157, see Fig.1(a)). Electronic band structure calculations^{23,24} show that this compound has a Fermi surface containing multiple electron and hole sheets. Angle-resolved photoemission spectroscopy (ARPES)^{25,26} and quantum oscillation studies²³ have measured the band structure and the Fermi surface. In particular, the ARPES data²⁶ revealed a spin-polarized surface state with linear dispersion, which was associated with the linear MR reported in an early study²⁷.

Here, we make detailed measurements of the angular dependent MR up to 22 T on a high quality single crystal of γ -PtBi₂. To analyze effects only due to the crystalline orientation to the magnetic field, we keep the field direction perpendicular to the electrical current. We observe a continuous evolution from a saturating sublinear MR for $\mathbf{B} \parallel \mathbf{c}$ to a nonsaturating quadraticlike MR for the field on the plane. The linear nonsaturating MR is only observed for a specific angle of the magnetic field with respect to the c axis. We show that such a linear MR appears at a specific angle in the presence of open orbits.

We grew single crystals of γ -PtBi₂²⁸ using the Bi self-flux method described in Ref.23. We used the equipment described in Ref.29, in particular, frit crucibles³⁰. Powder x-ray diffraction of our crystals reveals the expected crystal structure (Fig.1(b)), together with some peaks corresponding to residual Bi flux and Bi oxides. We measured a neat γ -PtBi₂ single crystal platelet, oriented with the \mathbf{c} -axis out of the plane (inset of Fig. 1(b)). The residual resistance ratio is of 100, showing excellent sample quality. To measure the MR, we used a cryostat capable of reaching about 1 K³¹, and a 20+2 T superconducting magnet supplied by Oxford Instruments³². We used a homemade mechanical rotator, described in the Supplemental Material³³, to modify the field angle. The current was applied perpendicular to the magnetic field (inset in Fig.1(c)). The rotator allowed an angular range covering from the field along the c axis ($\theta = 0^\circ$) to parallel to the plane ($\theta = 90^\circ$). The angle of the magnetic field was mea-

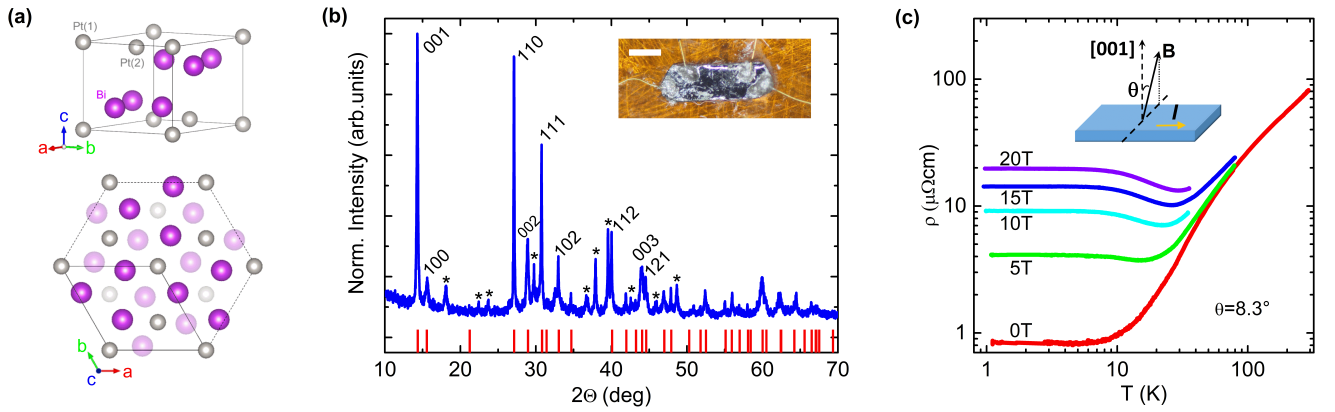


FIG. 1. (a) Crystal structure of the layered γ -PtBi₂. (b) In blue we show the x-ray diffraction pattern of γ -PtBi₂ powder. Red bars show the positions of the peaks expected to appear in this compound. The asterisks mark the peaks associated with residual Bi and Bi oxides from flux growth. The inset shows a picture of the single crystal with four contacts used for resistivity measurements. The white scale bar is 0.2 mm long. (c) Colored lines show the temperature dependence of the resistivity at different magnetic fields. The field is applied at an angle $\theta = 8.3^\circ$, which is also the precise angle at which we find nonsaturating linear magnetoresistance. The temperature dependence is very similar for all field orientations. The inset shows a scheme of the direction of the applied current and magnetic field.

sured using a Hall probe³⁴. We define $MR = \frac{\rho(B) - \rho(0)}{\rho(0)}$ with $\rho(0)$ being the resistivity at zero magnetic field, and provide it in percentage. To find Shubnikov de Haas oscillations, we obtain the oscillatory component ΔMR by fitting the MR data above 13 T to a low order polynomial and perform the Fourier transform of $\Delta MR(1/B)$.

Fig. 1(c) shows the resistivity as a function of temperature at different magnetic fields. We find a metallic behavior at zero field and a semiconductinglike behavior under magnetic fields (resistivity increases with decreasing temperature at low temperatures). The semiconductinglike increase saturates below about 8 K.

Fig. 2 shows the transverse MR up to 20 T for different orientations of the magnetic field, from $\mathbf{B} \parallel \mathbf{c}$ ($\theta = 0^\circ$) to $\mathbf{B} \perp \mathbf{c}$ ($\theta = 90^\circ$). The highest value of the MR is of 5800% at 20 T for θ close to 90° . For magnetic fields below 5 T, we always find a quadratic MR. For higher fields, we observe an angular evolution of the MR, from a concave curvature (saturating MR) at $\theta = 0^\circ$ to a quadraticlike, convex curvature (nonsaturating MR) at θ close to 90° . The magnitude of the MR changes by a factor of 5 as a function of the angle at high magnetic fields. In between the concave and convex magnetic field dependencies we observe a perfectly linear MR at $\theta = 8.3^\circ$.

To see this, we fit the data above 5 T with an empirical power law $MR(B) = c + aB^\alpha$. We find an increasing α with θ (inset of Fig. 2) up to 1.65. At $\theta = 8.3^\circ$, $\alpha = 1$ and the MR changes from saturating to non-saturating behavior.

Fig. 3(a) shows the quantum oscillation pattern in the MR for $\theta = 8.3^\circ$ as a function of the magnetic field. Fig. 3(b-d) present the Fourier transform of the quantum oscillation signal as a function of θ . Each quantum oscillation frequency F is related to an extremal cross-sectional area of the Fermi surface normal to the field

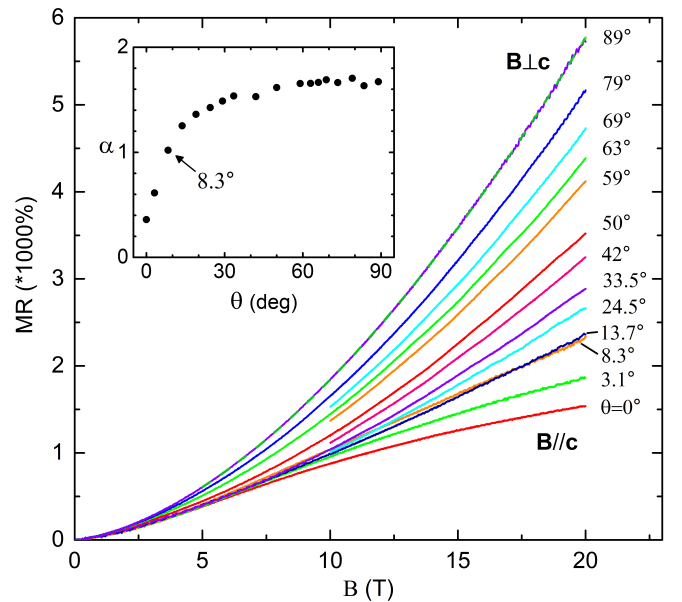


FIG. 2. MR up to 20 T for different field directions from $\mathbf{B} \parallel \mathbf{c}$ ($\theta = 0^\circ$) to $\mathbf{B} \perp \mathbf{c}$ (θ close to 90°). The inset shows the angular dependence of the exponent α obtained by fitting the MR at each angle with an empirical power law $MR = c + aB^\alpha$. The green broken line in the main figure shows, as an example, the fit for the data at $\theta = 89^\circ$.

\mathcal{A}_k through the Onsager relation, $F = (\hbar/2\pi e)\mathcal{A}_k$. In Fig. 3(e), we track the quantum oscillation frequencies as a function of the angle. At θ close to 0° our result exactly coincides with the result in Ref. 23 (taken along the same field direction). We can thus identify several frequencies, $F_\beta = 388$ T, $F_\gamma = 1225$ T and $F_\eta = 3012$ T, using the same notation²³. The results for finite θ are new and we use the same notation extrapolating from $\theta = 0^\circ$. We

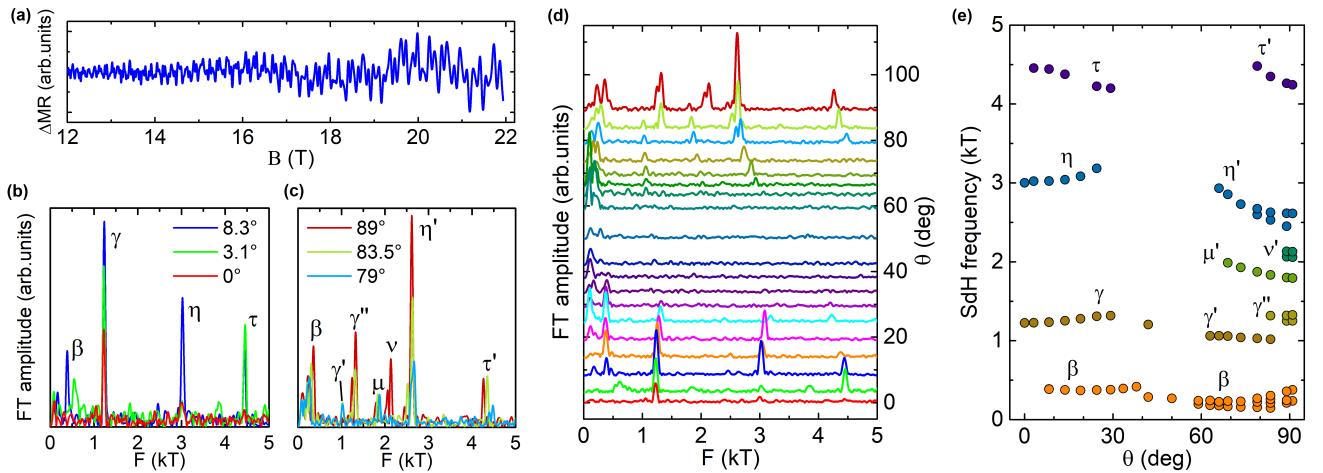


FIG. 3. (a) ΔMR (defined in the text) versus magnetic field up to 22 T at $T=1$ K and $\theta = 8.3^\circ$. (b,c) Fourier transform of ΔMR for a few values of θ . Greek letters mark the oscillation frequencies giving peaks in the Fourier transforms. (d) Fourier transform of ΔMR as a function of the frequency F for different θ . Data are shifted along the y -axis for clarity, following the value of θ 's. (e) Angular evolution of the quantum oscillations frequencies, with the corresponding orbits labeled by greek letters.

measure in a smaller field range than Ref.23. As a result two low frequency orbits (at 40 and at 15 T) are not well defined in our data. On the other hand we can sweep the magnetic field much more slowly and thus resolve better the high frequency quantum oscillations. For instance, we observe a high frequency oscillation around $F_\tau=4440$ T. The quantum oscillation pattern is very weak between $\theta = 30^\circ$ and 60° , so we cannot resolve the frequency of the orbits in this angular range, except for the orbit with the lowest frequency, β . We, thus, keep the notation for the orbits at θ close to 90° as for similar frequencies at θ close to 0° but add apostrophes. There are two extra frequencies that do not have direct counterparts at θ close to 0° , and we denote them as $F_{\mu'}=1798$ T and $F_{\nu'}=2012/2134$ T. Furthermore, we observe that η' , γ'' and ν' split into two and β into three frequencies close to 90° .

We have also measured the temperature dependence of the quantum oscillations at two different angles $\theta = 8.3^\circ$ and $\theta = 89^\circ$ where the oscillation amplitudes are the largest, to obtain the quasiparticle effective mass m_i^* of each orbit and their quantum lifetime τ_Q (see Fig.S1(a)-S1(c) and Table S1 in the Supplemental Material³³). m_i^* lies close to the free-electron mass m_e for all the orbits except β , whereas the estimated τ_Q ranges from 0.15 to 0.75 ps. We also analyze the phase of the lowest-frequency mode (β) and obtain, for this orbit, a nontrivial Berry phase Φ_B close to π . This result is in agreement with previous quantum oscillation measurements and suggests that the predicted triply degenerate point in the associated β band is likely to be present²³.

Band structure calculations in γ -PtBi₂^{23,35} show many bands that cross the Fermi level, forming six or seven sheets. Spin orbit coupling leads to large band splittings and the shape of the Fermi surface pockets is very sen-

sitive to the position of the Fermi level. At the Fermi level, the bands have mixed electron-hole character with a somewhat larger density of holes^{25,26}. We see that the smallest k_F (β orbit) in our quantum oscillation data is about 1/4 of the size of the first Brillouin zone and appears in pockets centered at the corners of the Brillouin zone derived from the β band²³. The two high-frequency orbits (η and τ) are associated with the two bands producing large pancakelike Fermi-surface sheets centered at the top and the bottom of the Brillouin zone²³. This particular shape gives extremal orbits only when $\mathbf{B} \parallel \mathbf{c}$ or $\perp \mathbf{c}$, which explains the absence of corresponding frequencies at intermediate angles. We also find several orbits split into two or more frequencies at θ close to 90° . This probably comes from the warping of the corresponding Fermi-surface sheets³⁶.

The calculations in Ref.23 reveal a γ band that has spherically-like Fermi-surface pockets arranged in a honeycomb lattice located on the plane and interconnected with each other through tilted necks. The lower inset of Fig. 4 presents schematically this open Fermi surface sheet. We mark, by the red dashed lines, two planes perpendicular to a magnetic field tilted from the c axis. These contain open orbits. In each of the planes, the spheres located at one side of the honeycomb structure are connected to each other, but not with the spheres of the other side (upper left insets of Fig. 4). Electrons on open orbits go into non-circular trajectories, instead of following cyclotron motion^{1,37}. This has a strong impact on the MR^{1,37-39}. In a metal with a single electronic band, open orbits lead to a quadratic enhancement of the MR at certain field angles, leaving a usual saturated MR at the angles where the open orbits are absent^{40,41}. Multiple Fermi-surface sheets as in γ -PtBi₂ are considered in detail here. To set up a MR model taking into account

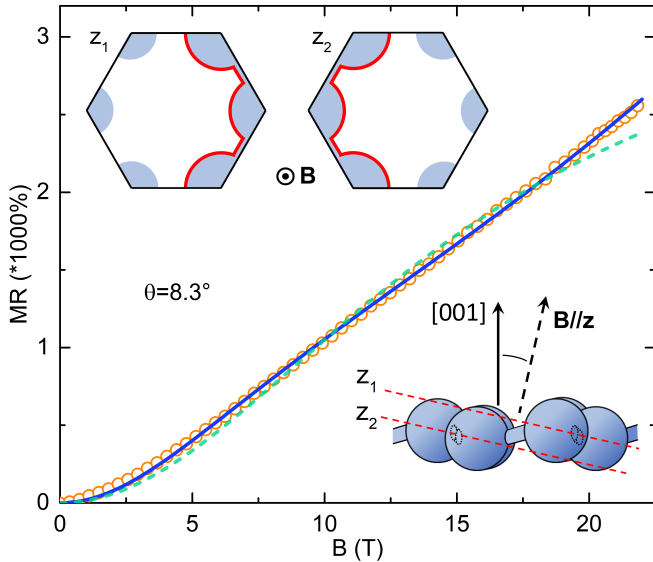


FIG. 4. We show as orange circles the MR at $\theta = 8.3^\circ$ up to 22 T. By the blue line we show the result of the model discussed in the text. The green dashed line shows the result of the same model, but without contribution from open orbits. Note the saturation observed at high magnetic fields. In the lower right inset, we show schematically the γ -band Fermi surface sheet. The shape is that of an undulated grid of spheres arranged in a honeycomb lattice perpendicular to the \mathbf{c} axis²³. The sheets are connected by necks oriented at an angle to the plane. Necks that lie behind the spheres are schematically represented by dashed lines. When the magnetic-field direction is slightly tilted from \mathbf{c} , open orbits may appear on two different planes (marked by red dashed lines). The corresponding open orbits are provided in the upper left panels.

multiple sheets, we first consider that, in a semimetal, the MR has a B^2 unsaturated behavior when the electron and hole numbers (n_e and n_h) are compensated^{1,7,42}. We consider a two-band model and take electrons as free carriers with the same mobility μ . The level of electron-hole compensation is given by $d = (n_e - n_h)/(n_e + n_h)$. We add a field-independent small contribution from the open orbits $\delta\sigma_0$ to the total conductivity σ_0 . More details are provided in the Supplemental Material³³. We can then write for the resistivity $\rho(B)/\rho_0 = \frac{\delta(1+\eta^2)^2 + (1+\eta^2)}{\delta(1+\eta^2) + 1 + d^2\eta^2}$, where $\eta = \mu B$.

We find that this reproduces nicely the linear MR at 8.3° (Fig. 4) and at all other field orientations (see Fig. S2 in the Supplemental material³³). We use for this angle the parameters $\delta = 0.00849$, $\mu = 4630 \text{ cm}^2\text{V}^{-1}\text{s}^{-1}$ and $|d| = 0.229$. The size of δ is small compared to one, in agreement with the fact that only a tiny proportion of the whole Fermi surface would be engaged in forming open orbits. From the mobility μ , we estimate the transport mean free scattering time τ_{tr} ($\mu = e\tau_{tr}/m^*$) to be around $2.6 \cdot 10^{-12}\text{s}$, a few times larger than the quantum lifetime τ_Q deduced from the amplitude of the quantum oscillations (Table S1 in the Supplemental Material³³). This difference is reasonable as τ_Q measures the smearing of

the Landau levels due to forward and backward scatterings, whereas transport τ_{tr} requires backscattering. The linear MR cannot be obtained without taking into account the open orbits (δ term), and the MR would show a clear saturation at high fields due to an inexact compensation between the electron and the hole carrier numbers. It is, thus, the combination of both effects that leads to the observed linear MR at $\theta = 8.3^\circ$. For the other angles, we can associate the increase in the MR from 0° to 90° and the evolution of its curvature to changes in $|d|$, which steadily decreases from 0.22 at 0° to close to 0 at 90° .

The relevant contribution of a one-dimensional conduction channel for the magnetoresistance which we unveil here can have consequences, particularly, for the behavior at even larger magnetic fields. The Lebed effect consists of resonances occurring in open orbits for in- and out-of-plane transport between layers of a two-dimensional crystalline structure⁴³. As a consequence, different kinds of oscillatory behavior related to open orbits have been predicted and observed in organic systems, including magic angles related to dimensional crossovers, strong angular-dependent oscillations, or density waves⁴⁴⁻⁴⁷. Our result suggests that such one-dimensional features could arise in semimetals due to open orbits.

This seems particularly interesting in view of the unconventional bandstructures often observed in semimetals. For γ -PtBi₂, band structure calculations suggest triply degenerate nodal points^{20,21,23,26}. Contrary to Dirac and Weyl fermions^{23,35,48,49}, triple points have no counterpart in high energy physics^{35,48-50}. These could influence the magnetoresistance in the case of complex conduction paths involving open orbits induced by the magnetic field.

To summarize, we synthesized high quality single crystals of γ -PtBi₂ and measured the angular dependence of the MR up to 22 T. We reveal that, in addition to the known electron-hole compensation, open orbits produce an important modification of the transport under magnetic fields leading to huge values of the magnetoresistance and a linear field dependence. Additionally, we suggest that phenomena inherent to one-dimensional conduction might appear at ultra high magnetic fields in low carrier density semimetals.

ACKNOWLEDGEMENTS

This work was supported by the European Research Council PNICTEYES Grant Agreement No. 679080, by the Spanish Research State Agency (Grants No. FIS2017-84330-R, No. CEX2018-000805-M, and No. RYC-2014-15093) and by the Comunidad de Madrid through Program NANOMAGCOST-CM (Program No. S2018/NMT-4321). We acknowledge collaborations through the EU program Cost CA16218 (NanocoHybri). We particularly acknowledge SEGAINVEX at UAM for design and construction of cryogenic equipment. We also thank R. Álvarez Montoya and J.M. Castilla for techni-

cal support and S. Delgado for support with the single crystal growth. We learned of the search for new ma-

terials with P. C. Canfield and are very grateful to him for this. We acknowledge SIDI at UAM for support in sample characterization.

- ¹ A. Pippard, *Magnetoresistance in Metals*, Cambridge Studies in Low Temperature Physics (Cambridge University Press, 1989).
- ² A. Abrikosov, *Fundamentals of the Theory of Metals* (Dover Publications, 2017).
- ³ P. Kapitza, *The change of electrical conductivity in strong magnetic fields. Part I. Experimental results*, *Proc. R. Soc. London, Ser. A* **123**, 292341 (1929).
- ⁴ Z. Zhu, B. Fauqué, K. Behnia, and Y. Fuseya, *Magnetoresistance and valley degree of freedom in bulk bismuth*, *Journal of Physics: Condensed Matter* **30**, 313001 (2018).
- ⁵ P. B. Alers and R. T. Webber, *The magnetoresistance of bismuth crystals at low temperatures*, *Phys. Rev.* **91**, 1060 (1953).
- ⁶ F. Y. Yang, K. Liu, C. L. Chien, and P. C. Searson, *Large magnetoresistance and finite-size effects in electrodeposited single-crystal Bi thin films*, *Phys. Rev. Lett.* **82**, 3328 (1999).
- ⁷ M. N. Ali, J. Xiong, S. Flynn, J. Tao, Q. D. Gibson, L. M. Schoop, T. Liang, N. Haldolaarachchige, M. Hirschberger, N. P. Ong, and R. J. Cava, *Large, non-saturating magnetoresistance in WTe_2* , *Nature* **514**, 205 EP (2014).
- ⁸ F. F. Tafti, Q. D. Gibson, S. K. Kushwaha, N. Haldolaarachchige, and R. J. Cava, *Resistivity plateau and extreme magnetoresistance in $LaSb$* , *Nature Physics* **12**, 272 EP (2015).
- ⁹ Y. Feng, Y. Wang, D. M. Silevitch, J.-Q. Yan, R. Kobayashi, M. Hedo, T. Nakama, Y. Onuki, A. V. Suslov, B. Mihaila, P. B. Littlewood, and T. F. Rosenbaum, *Linear magnetoresistance in the low-field limit in density-wave materials*, *Proceedings of the National Academy of Sciences* **116**, 11201 (2019).
- ¹⁰ I. A. Leahy, Y.-P. Lin, P. E. Siegfried, A. C. Treglia, J. C. W. Song, R. M. Nandkishore, and M. Lee, *Nonsaturating large magnetoresistance in semimetals*, *Proceedings of the National Academy of Sciences* **115**, 10570 (2018).
- ¹¹ S. Mitra, J. G. S. Kang, J. Shin, J. Q. Ng, S. S. Sunku, T. Kong, P. C. Canfield, B. S. Shastry, P. Sengupta, and C. Panagopoulos, *Quadratic to linear magnetoresistance tuning in TmB_4* , *Phys. Rev. B* **99**, 045119 (2019).
- ¹² S. L. Bud'ko, P. C. Canfield, C. H. Mielke, and A. H. Lacerda, *Anisotropic magnetic properties of light rare-earth diantimonides*, *Phys. Rev. B* **57**, 13624 (1998).
- ¹³ K. Myers, S. Bud'ko, I. Fisher, Z. Islam, H. Kleinke, A. Lacerda, and P. Canfield, *Systematic study of anisotropic transport and magnetic properties of $RAgSb_2$ ($R=Y, La-Nd, Sm, Gd-Tm$)*, *Journal of Magnetism and Magnetic Materials* **205**, 27 (1999).
- ¹⁴ E. Mun, H. Ko, G. J. Miller, G. D. Samolyuk, S. L. Bud'ko, and P. C. Canfield, *Magnetic field effects on transport properties of $PtSn_4$* , *Phys. Rev. B* **85**, 035135 (2012).
- ¹⁵ Y. Wu, L.-L. Wang, E. Mun, D. D. Johnson, D. Mou, L. Huang, Y. Lee, S. L. Bud'ko, P. C. Canfield, and A. Kaminski, *Dirac node arcs in $PtSn_4$* , *Nature Physics* **12**, 667 EP (2016).
- ¹⁶ R. F. Luccas, A. Fente, J. Hanko, A. Correa-Orellana, E. Herrera, E. Climent-Pascual, J. Azpeitia, T. Pérez-Castañeda, M. R. Osorio, E. Salas-Colera, N. M. Nemes, F. J. Mompean, M. García-Hernández, J. G. Rodrigo, M. A. Ramos, I. Guillamón, S. Vieira, and H. Suderow, *Charge density wave in layered $La_{1-x}Ce_xSb_2$* , *Phys. Rev. B* **92**, 235153 (2015).
- ¹⁷ J. A. Galvis, H. Suderow, S. Vieira, S. L. Bud'ko, and P. C. Canfield, *Scanning tunneling microscopy in the superconductor $LaSb_2$* , *Phys. Rev. B* **87**, 214504 (2013).
- ¹⁸ H.-Y. Yang, T. Nummy, H. Li, S. Jaszewski, M. Abramchuk, D. S. Dessau, and F. Tafti, *Extreme magnetoresistance in the topologically trivial lanthanum monopnictide $LaAs$* , *Phys. Rev. B* **96**, 235128 (2017).
- ¹⁹ C. Shekhar, A. K. Nayak, Y. Sun, M. Schmidt, M. Nicklas, I. Leermakers, U. Zeitler, Y. Skourski, J. Wosnitza, Z. Liu, Y. Chen, W. Schnelle, H. Borrmann, Y. Grin, C. Felser, and B. Yan, *Extremely large magnetoresistance and ultra-high mobility in the topological Weyl semimetal candidate NbP* , *Nature Physics* **11**, 645 EP (2015).
- ²⁰ B. Q. Lv, Z.-L. Feng, Q.-N. Xu, X. Gao, J.-Z. Ma, L.-Y. Kong, P. Richard, Y.-B. Huang, V. N. Strocov, C. Fang, H.-M. Weng, Y.-G. Shi, T. Qian, and H. Ding, *Observation of three-component fermions in the topological semimetal molybdenum phosphide*, *Nature* **546**, 627 EP (2017).
- ²¹ J.-Z. Ma, J.-B. He, Y.-F. Xu, B. Q. Lv, D. Chen, W.-L. Zhu, S. Zhang, L.-Y. Kong, X. Gao, L.-Y. Rong, Y.-B. Huang, P. Richard, C.-Y. Xi, E. S. Choi, Y. Shao, Y.-L. Wang, H.-J. Gao, X. Dai, C. Fang, H.-M. Weng, G.-F. Chen, T. Qian, and H. Ding, *Three-component fermions with surface Fermi arcs in tungsten carbide*, *Nature Physics* **14**, 349 (2018).
- ²² N. H. Jo, Y. Wu, L.-L. Wang, P. P. Orth, S. S. Downing, S. Manni, D. Mou, D. D. Johnson, A. Kaminski, S. L. Bud'ko, and P. C. Canfield, *Extremely large magnetoresistance and Kohler's rule in $PdSn_4$: A complete study of thermodynamic, transport, and band-structure properties*, *Phys. Rev. B* **96**, 165145 (2017).
- ²³ W. Gao, X. Zhu, F. Zheng, M. Wu, J. Zhang, C. Xi, P. Zhang, Y. Zhang, N. Hao, W. Ning, and M. Tian, *A possible candidate for triply degenerate point fermions in trigonal layered $PtBi_2$* , *Nature Communications* **9**, 3249 (2018).
- ²⁴ C. Q. Xu, X. Z. Xing, X. Xu, B. Li, B. Chen, L. Q. Che, X. Lu, J. Dai, and Z. X. Shi, *Synthesis, physical properties, and band structure of the layered bismuthide $PtBi_2$* , *Phys. Rev. B* **94**, 165119 (2016).
- ²⁵ Q. Yao, Y. P. Du, X. J. Yang, Y. Zheng, D. F. Xu, X. H. Niu, X. P. Shen, H. F. Yang, P. Dudin, T. K. Kim, M. Hoesch, I. Vobornik, Z.-A. Xu, X. G. Wan, D. L. Feng, and D. W. Shen, *Bulk and surface electronic structure of hexagonal structured $PtBi_2$ studied by angle-resolved photoemission spectroscopy*, *Phys. Rev. B* **94**, 235140 (2016).
- ²⁶ S. Thirupathiah, Y. Kushnirenko, E. Haubold, A. V. Fedorov, E. D. L. Rienks, T. K. Kim, A. N. Yaresko, C. G. F. Blum, S. Aswartham, B. Büchner, and S. V. Borisenko,

- Possible origin of linear magnetoresistance: Observation of Dirac surface states in layered $PtBi_2$, *Phys. Rev. B* **97**, 035133 (2018).
- ²⁷ X. Yang, H. Bai, Z. Wang, Y. Li, Q. Chen, J. Chen, Y. Li, C. Feng, Y. Zheng, and Z.-a. Xu, *Giant linear magnetoresistance in nonmagnetic $PtBi_2$* , *Applied Physics Letters* **108**, 252401 (2016).
- ²⁸ N. Zhuravlev and L. Kertes, *Structure of superconductors. XI. investigation of alloys of bismuth with platinum, ruthenium, osmium and iridium.*, *JETP* **5** (1957).
- ²⁹ P. C. Canfield and Z. Fisk, *Growth of single crystals from metallic fluxes*, *Philosophical Magazine B* **65**, 1117 (1992).
- ³⁰ P. C. Canfield, T. Kong, U. S. Kaluarachchi, and N. H. Jo, *Use of frit-disc crucibles for routine and exploratory solution growth of single crystalline samples*, *Philosophical Magazine* **96**, 84 (2016).
- ³¹ R. A. Montoya, S. Delgado, J. Castilla, J. Navarrete, N. D. Contreras, J. R. Marijuan, V. Barrena, I. Guillamón, and H. Suderow, *Methods to simplify cooling of liquid helium cryostats*, *HardwareX* **5**, e00058 (2019).
- ³² *Commissioning note by Oxford Instruments.*
- ³³ See Supplemental Material for (i) details of the analyses of the Shubnikov-de Haas quantum oscillations, (ii) a detailed semi-classical model taking into account the open orbits to explain the magnetoresistance in the whole angular range, (iii) angular dependence of the magnetoresistance, and (iv) description of the mechanical rotator set-up for resistivity measurements.
- ³⁴ *Hall probes from Arepok.*
- ³⁵ H. Weng, C. Fang, Z. Fang, and X. Dai, *Coexistence of Weyl fermion and massless triply degenerate nodal points*, *Phys. Rev. B* **94**, 165201 (2016).
- ³⁶ A. Carrington, J. D. Fletcher, and H. Harima, *Interpretation of the angular dependence of the de Haas-van Alphen effect in MgB_2* , *Phys. Rev. B* **71**, 174505 (2005).
- ³⁷ I. Lifshitz, M. I. Azbel, and M. Kaganov, *The theory of galvanomagnetic effects in metals*, *JETP* **4**, 41 (1957).
- ³⁸ I. Lifshitz and V. G. Peschanskii, *Galvanomagnetic characteristics of metals with open Fermi surfaces.I*, *JETP* **8**, 875 (1959).
- ³⁹ I. Lifshitz and V. G. Peschanskii, *Galvanomagnetic characteristics of metals with open Fermi surfaces.II*, *JETP* **11**, 137 (1960).
- ⁴⁰ J. R. Klauder, W. A. Reed, G. F. Brennert, and J. E. Kunzler, *Study of the fine structure in the high-field galvanomagnetic properties and the Fermi surface of copper*, *Phys. Rev.* **141**, 592 (1966).
- ⁴¹ M. Huberman and A. W. Overhauser, *Open-orbit magnetoresistance spectra of potassium*, *Phys. Rev. B* **25**, 2211 (1982).
- ⁴² W. Gao, N. Hao, F.-W. Zheng, W. Ning, M. Wu, X. Zhu, G. Zheng, J. Zhang, J. Lu, H. Zhang, C. Xi, J. Yang, H. Du, P. Zhang, Y. Zhang, and M. Tian, *Extremely large magnetoresistance in a topological semimetal candidate pyrite $PtBi_2$* , *Phys. Rev. Lett.* **118**, 256601 (2017).
- ⁴³ A. G. Lebed and P. Bak, *Theory of unusual anisotropy of magnetoresistance in organic superconductors*, *Phys. Rev. Lett.* **63**, 1315 (1989).
- ⁴⁴ P. Dhakal, H. Yoshino, J. I. Oh, K. Kikuchi, and M. J. Naughton, *Observation and simulation of all angular magnetoresistance oscillation effects in the quasi-one-dimensional organic conductor $(DMET)_2I_3$* , *Phys. Rev. Lett.* **105**, 067201 (2010).
- ⁴⁵ A. G. Lebed, N. N. Bagmet, and M. J. Naughton, *Magic angle effects and angular magnetoresistance oscillations as dimensional crossovers*, *Phys. Rev. Lett.* **93**, 157006 (2004).
- ⁴⁶ G. M. Danner, W. Kang, and P. M. Chaikin, *Measuring the Fermi surface of quasi-one-dimensional metals*, *Phys. Rev. Lett.* **72**, 3714 (1994).
- ⁴⁷ T. Osada and E. Ohmichi, *Magnetotransport and magnetic-field-induced density waves in low-dimensional layered conductors*, *Journal of the Physical Society of Japan* **75**, 051006 (2006).
- ⁴⁸ B. Bradlyn, J. Cano, Z. Wang, M. G. Vergniory, C. Felser, R. J. Cava, and B. A. Bernevig, *Beyond Dirac and Weyl fermions: Unconventional quasiparticles in conventional crystals*, *Science* **353** (2016).
- ⁴⁹ G. Chang, S.-Y. Xu, S.-M. Huang, D. S. Sanchez, C.-H. Hsu, G. Bian, Z.-M. Yu, I. Belopolski, N. Alidoust, H. Zheng, T.-R. Chang, H.-T. Jeng, S. A. Yang, T. Neupert, H. Lin, and M. Z. Hasan, *Nexus fermions in topological symmorphic crystalline metals*, *Scientific Reports* **7**, 1688 (2017).
- ⁵⁰ A. Ramires and J. L. Lado, *Impurity-induced triple point fermions in twisted bilayer graphene*, *Phys. Rev. B* **99**, 245118 (2019).

Supplemental Materials for “Huge linear magnetoresistance due to open orbits in γ -PtBi₂”

I. TEMPERATURE AND FIELD DEPENDENCE OF THE SHUBNIKOV-DE HAAS OSCILLATIONS

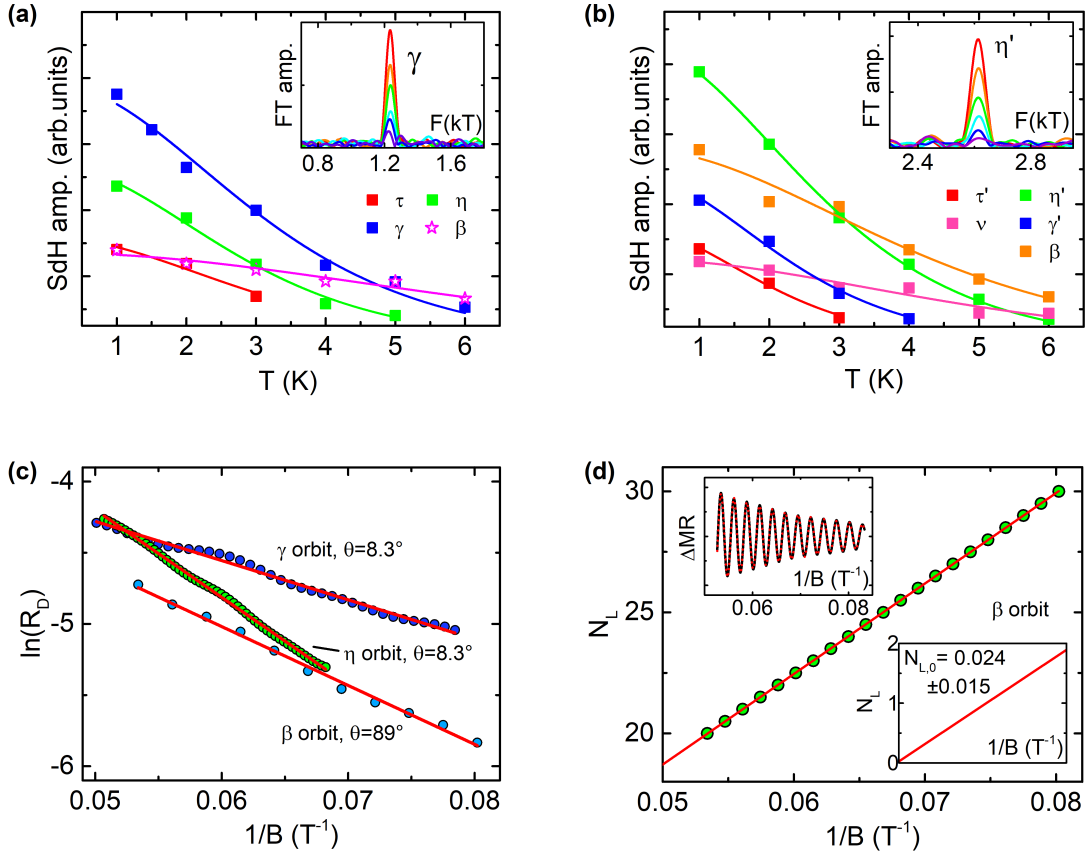


FIG. S1. (a,b) We show as points the amplitude of the quantum oscillations of different frequencies observed at $\theta = 8.3^\circ$ and $\theta = 89^\circ$ as a function of temperature. Lifshitz-Kosevich fits are shown as solid lines. Each of the insets shows one of the Fourier transform peaks in the quantum oscillations with increasing temperature, from T=1 K (red) to 6 K (blue). (c) We show as points the Dingle factor R_D (in a logarithmic scale) as a function of $1/B$ for a few selected frequencies (γ at $\theta = 8.3^\circ$, blue points, η at the same angle, green points and β at $\theta = 89^\circ$, light blue points). The red lines are linear fits to each magnetic field dependence. (d) Landau level index (N_L) as a function of $1/B$ extracted from the peaks (integer) and valleys (half integer) for one of the β orbits at 89° . The solid line is a linear fit. The lower right inset shows the zero $1/B$ intercept, giving $N_{L,0} = 0.024 \pm 0.015$. The upper left inset shows the amplitude of quantum oscillations with frequency F_β vs $1/B$ obtained by band-pass filtering the raw data (black points are the data and red dotted line the fit to LK formula) and used to obtain N_L .

To discuss the temperature and magnetic field dependence of the amplitude of the quantum oscillations, let us write down the Lifshitz-Kosevich formula:

$$\Delta MR \propto \sqrt{B} \frac{\Theta m_i^* T/B}{\sinh(\Theta m_i^* T/B)} \exp(-\Theta m_i^* T_D/B) \cos \left[2\pi \left(\frac{F}{B} + \gamma - \delta \right) \right] \quad (S1)$$

where ΔMR is the oscillatory component of the MR, m_i^* the effective electron mass of band i , $\Theta = 2\pi^2 k_B / e\hbar$ is a numerical factor and $T_D = \hbar / 2\pi k_B \tau_Q$ is the Dingle temperature. The phase factor $\cos [2\pi (\frac{F}{B} + \gamma - \delta)]$ depends on the frequency F (normalized to B), on the phase shift δ , given by the dimensionality of the Fermi surface (equal to 0 in a 2D system and $\pm 1/8$ in 3D) and on the phase shift γ . γ is related to the Berry phase Φ_B accumulated over the orbit as $\gamma = \frac{1}{2} - \frac{\Phi_B}{2\pi}$.

In Fig. S1(a,b) we show the temperature dependence of the amplitude of the Fourier transforms of the quantum oscillations at 8.3° and 89° , respectively. We obtain the quasiparticle effective mass m_i^* of each orbit from the fits

to equation S1. In Fig.S1(c) we show the Dingle factor $R_D = \exp(-\Theta m_i^* T_D/B)$ as a function of $1/B$ for a few selected frequencies. From these fits, we obtain the quantum lifetime τ_Q in each band. The resulting parameters are summarized in Table S1. The Fermi wavevector k_F is calculated from the frequency F with the Onsager relation and the assumption of a circular orbit: $\mathcal{A} = \pi k_F^2$. We see that k_F spans a large part of the Brillouin zone. The electron effective mass m_i^* is very close to the free electron mass for nearly all orbits, except for the β orbit where it is considerably smaller, about $0.4m_e$, in good agreement with previous quantum oscillation measurements¹. The mean free path ℓ ranges from 400 Å to about 4000 Å.

TABLE S1. Fermi surface parameters obtained from the quantum oscillations for two particular angular orientations of the magnetic field. F is the frequency, k_F the Fermi wavevector, m^* the effective mass, $\ell(\text{Å})$ the quantum mean free path and τ_Q the quantum lifetime.

		F(T)	$k_F(\text{nm}^{-1})$	m^*/m_e	$\ell(\text{Å})$	$\tau_Q(\text{ps})$
8.3°	β	388	1.09	0.39 ± 0.03	420	0.14
	γ	1235	1.94	0.77 ± 0.01	1500	0.51
	η	3023	3.03	0.90 ± 0.03	1020	0.26
	τ	4442	3.67	0.83 ± 0.04	3770	0.73
89°	β	377	1.04	0.61 ± 0.03	520	0.26
	γ'	1323	2.00	1.00 ± 0.01	1070	0.46
		1248	1.95	0.89 ± 0.01		
	ν	2132	2.55	0.52 ± 0.01	870	0.15
	η'	2615	2.82	0.87 ± 0.03	1400	0.37
	τ'	4326	3.60	0.98 ± 0.04	760	0.22

If a non-trivial Berry phase π is acquired over an orbit, a change in γ will occur and the phase of the quantum oscillations will be shifted. In such case, in the linear plot of the Landau index N_L versus $1/B$, the zero $1/B$ intercept of N_L will lie close to 0. In case of a topologically trivial band with no Berry phase accumulation, the zero $1/B$ intercept of N_L will lie inside the interval $[3/8, 5/8]$. In the upper left inset of Fig.S1(d) we show the oscillation of the β -orbit at 89° ($F=377$ T). Fig.S1(d) shows the Landau index N_L plotted as a function of the maximum and minimum position in $1/B$ for this orbit. The zero $1/B$ extrapolation (lower right inset) gives an intercept $N_{L,0} = 0.024 \pm 0.015$, a value quite close to zero.

II. TWO-BAND ISOTROPIC MODEL INCLUDING CONTRIBUTION FROM OPEN ORBITS

Let the \mathbf{z} -axis be along the direction of the applied magnetic field. Semiclassically, for a free electron gas, the resistivity tensor in the transverse plane (\mathbf{x}, \mathbf{y}) can be written as:

$$\hat{\rho} = \begin{pmatrix} \frac{1}{\sigma_e} & \frac{\eta_e}{\sigma_e} \\ \frac{\eta_e}{\sigma_e} & \frac{1}{\sigma_e} \end{pmatrix} \quad (\text{S2})$$

where σ_e is the zero field conductivity and $\eta_e = \mu_e B$ with μ_e the electron mobility. In Equation S2, $\rho_{xx} = \rho_{yy}$, and it is independent of magnetic field. The corresponding conductivity tensor is the following:

$$\hat{\sigma}_e = \begin{pmatrix} \frac{\sigma_e}{1 + \eta_e^2} & -\frac{\eta_e \sigma_e}{1 + \eta_e^2} \\ \frac{\eta_e \sigma_e}{1 + \eta_e^2} & \frac{\sigma_e}{1 + \eta_e^2} \end{pmatrix} \quad (\text{S3})$$

The conductivity tensor for an isotropic single band of hole carriers can be written in the same way, apart from an opposite sign in the off-diagonal terms. When both electrons and holes are present and considered as independent conduction channels, one needs to add them in the conductivity tensor:

$$\hat{\sigma} = \hat{\sigma}_e + \hat{\sigma}_h = \begin{pmatrix} \frac{\sigma_e}{1 + \eta_e^2} & -\frac{\eta_e \sigma_e}{1 + \eta_e^2} \\ \frac{\eta_e \sigma_e}{1 + \eta_e^2} & \frac{\sigma_e}{1 + \eta_e^2} \end{pmatrix} + \begin{pmatrix} \frac{\sigma_h}{1 + \eta_h^2} & \frac{\eta_h \sigma_h}{1 + \eta_h^2} \\ -\frac{\eta_h \sigma_h}{1 + \eta_h^2} & \frac{\sigma_h}{1 + \eta_h^2} \end{pmatrix} \quad (\text{S4})$$

Inverting $\hat{\sigma}$ leads to the field dependence of the resistivity ρ_{xx} (x being the current direction):

$$\rho_{xx} = \frac{n_e\mu_e + n_h\mu_h + \mu_e\mu_h(n_e\mu_h + n_h\mu_e)B^2}{e[(n_e\mu_e + n_h\mu_h)^2 + (n_e - n_h)^2\mu_e^2\mu_h^2B^2]} \quad (\text{S5})$$

where we have used the Drude formula for conductivity, $\sigma = ne\mu$. Equation S5 is a result discussed in Ref. 2. When the electron and hole carrier numbers come close to compensation, ρ_{xx} reaches a resonance and increases as B^2 without saturation.

In γ -PtBi₂, we can approximate the band structure by a two-band model. In our model, we consider one band which is fundamentally different from the others, due to the topology of its Fermi surface. It has an open Fermi surface formed by sphere-like sheets interconnected with each other, giving a 2D grid in reciprocal space. Electrons can be driven into open, non-circular orbits in the grid. The open orbits extend along the intersection line (along \mathbf{x} , the current direction) between the plane perpendicular to the field (\mathbf{x}, \mathbf{y}), and the [001] plane. Electron dynamics in open orbits is governed only by the usual scattering processes that are present without magnetic field. Thus they lead to an additional field-independent term in σ_{yy} . With this, we can write:

$$\hat{\sigma} = \begin{pmatrix} \frac{\sigma_0}{1 + \eta^2} & -\frac{d\eta\sigma_0}{1 + \eta^2} \\ \frac{d\eta\sigma_0}{1 + \eta^2} & \delta\sigma_0 + \frac{\sigma_0}{1 + \eta^2} \end{pmatrix} \quad (\text{S6})$$

where $\sigma_0 = \sigma_e + \sigma_h = (n_e + n_h)e\mu$ is the total conductivity at zero field. The two-band model is characterized by $d = (\sigma_e - \sigma_h)/\sigma_0 = (n_e - n_h)/(n_e + n_h)$. The contribution from the open orbits, $\sigma_{o.o.} = \delta \cdot \sigma_0$ is small ($\delta \ll 1$), as only a tiny proportion of the whole Fermi surface should be engaged in forming the open orbits. From Equation S6 we deduce the following expression used in the main text, by inverting the conductivity tensor:

$$\rho(B)/\rho_0 = \frac{\delta(1 + \eta^2)^2 + (1 + \eta^2)}{\delta(1 + \eta^2) + 1 + d^2\eta^2} \quad (\text{S7})$$

Fig. S2 (a) shows how Equation S7 can explain our MR data in the whole angular range. The classical two-band model without open orbit contributions (without δ terms in Equation S7) gives a good account for the MR behavior at most of the angles. In particular, it explains well both the saturating behavior at $\theta = 0^\circ$, and the quasi B^2 behavior at θ close to 90° . However, at θ around 8.3° , it is not possible to reproduce the observed linear or quasi linear MR with the two-band model alone. Notably, a pronounced saturating behavior in the high field limit would always appear in this model. Introducing a contribution from open orbits (δ terms in Equation S7) successfully reproduces the MR. In particular the linear MR at $\theta = 8.3^\circ$ is well explained. Fig. S2 (b) shows the angular evolution of the different parameters used in the fits. The steady increase of the MR with θ in the whole angular range, together with the reversal of the MR curvature, can be associated to a steady decrease of $|d|$ from 0.22 to 0.07 (the electron and hole number gradually approach compensation). The open orbits contribution to the conductivity δ equals 0 except at θ around 8.3° . The mobility μ undergoes little change with the angle.

III. ANGULAR DEPENDENCE OF THE MAGNETORESISTANCE

In Fig. S3 (a) we show the angular dependence of the MR at constant magnetic fields. We find a strong increase for θ close to 0° which ceases at about 8.3° , the angle at which the MR changes from a saturating to a non-saturating behavior. The dip turns into a MR(θ) consisting of a smooth background and a small oscillatory component for $\theta > 8.3^\circ$. We fit the background with a polynomial function of order 4 (dashed lines in Fig. S3(a)) and visualize the oscillatory dependence in Fig. S3(b). In Fig. S3(c) we plot the same data as a function of $\tan(\theta)$. We observe that the magnitude of the oscillations in $\Delta\text{MR}(\theta)$ increases with the magnetic field. Their position in θ , however, is independent of the magnetic field. Notice that Shubnikov-de Haas quantum oscillations may provide oscillations in the angular dependence of the MR. However, their positions in angle should depend on the field, which is not the case here. Moreover, the amplitude of quantum oscillations in our data is one order of magnitude smaller than the oscillating pattern in the angular dependence of the MR, as we can see in the inset of Fig. S3(c).

Angular dependent MR oscillations, whose position in θ does not change with the magnetic field, have been obtained in a number of systems³⁻¹¹. In particular, in layered materials, MR oscillations appear due to two-dimensional Fermi surface sheets with some warping^{10,11}. Two-dimensional Fermi surface tubes without warping only have one orbit for the magnetic field applied exactly parallel to the tube. By contrast, tubes with a small amount of warping show

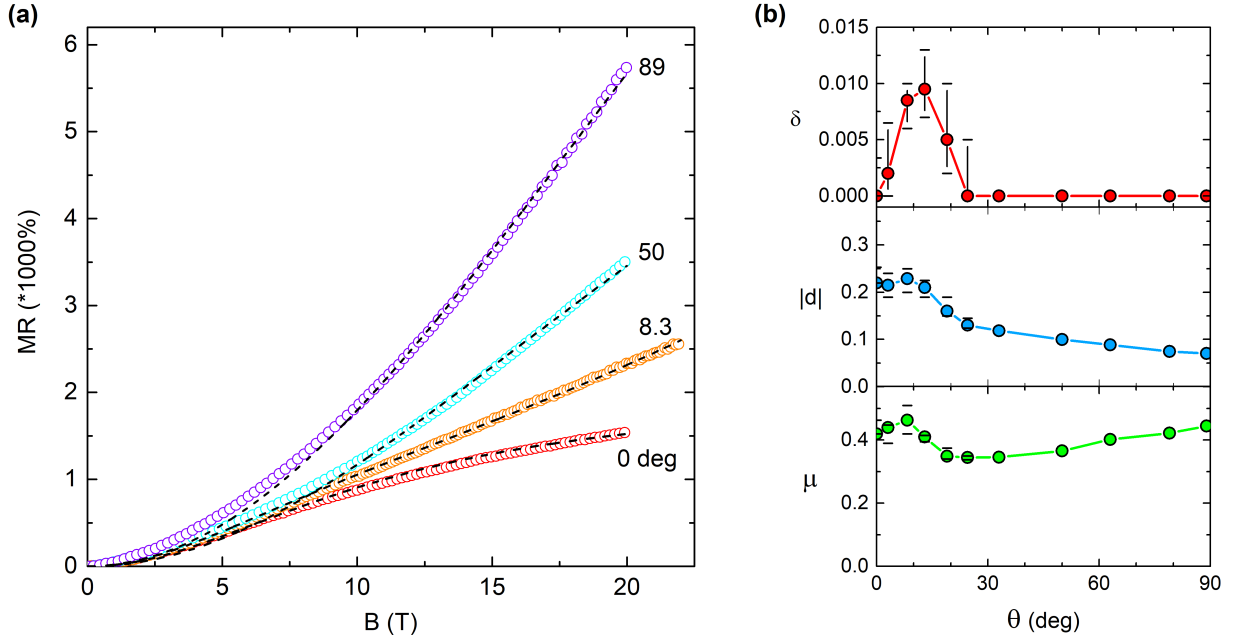


FIG. S2. (a) The open circles show the MR data at different field orientations. The dashed lines show the corresponding fits to Equation S7. (b) Angular evolution of the used parameters. The contribution from the open orbits δ appears at θ close to 8.3° . The steady increase of the MR with θ in the whole angular range is mostly associated to a steady decrease of $|d|$ from 0.22 to 0.07 (gradual approaching to an exact electron-hole compensation).

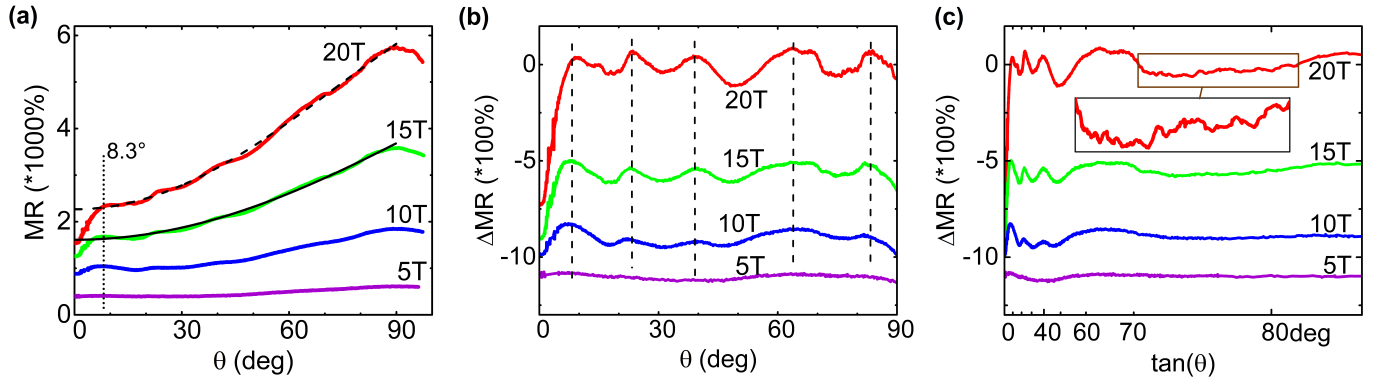


FIG. S3. (a) Angular dependence of the MR at different magnetic fields, at T=1 K. The vertical dotted line marks the angle where a linear MR is observed: $\theta = 8.3^\circ$. The black lines show pair polynomial fits of order 4 to remove the background and get the oscillating part in (b). (b) The oscillating part of the angular dependence of the MR at different magnetic fields, at T=1 K (shifted along the vertical axis for clarity). The dashed vertical lines are guides for the eyes, and show that the angles where we observe oscillations do not depend on the magnetic field. (c) ΔMR as a function of $\tan(\theta)$, at different magnetic fields. The inset gives a zoom on the signal in the MR due to quantum oscillations, which is strongly magnetic field dependent.

exactly two orbits defining two extremal areas of the Fermi surface for all orientations of the magnetic field. Yamaji showed that the difference between these extremal areas becomes zero at integer values of $\tan(\theta)$ ¹². It was then shown that this causes maxima in the angular dependent MR at angles corresponding to integer values of $\tan(\theta)$ ¹². Of course, this assumes that warping follows a spherical or cosine-like form along the \mathbf{c} -axis. In γ -PtBi₂, quantum oscillations do not show tube-like Fermi surface sheets associated with a 2D nature of a layered system, and there is no sign of them in calculations neither^{1,13}. Instead, they show 3D spherical-like Fermi surfaces sheets with complex geometries. Then the angular-dependent oscillations of the MR may come from a similar effect within a more complex band structure, associated with 3D Fermi surface sheets with a spherical-like geometry which provide orbits with exactly the same area for different angles $\tan(\theta)$. Thus, the origin of the angular dependent oscillations may come from coincidences in size between different orbits on 3D Fermi surface sheets at certain field orientations.

IV. DESCRIPTION OF THE MECHANICAL ROTATOR USED FOR THE ANGULAR DEPENDENT MAGNETORESISTANCE MEASUREMENTS

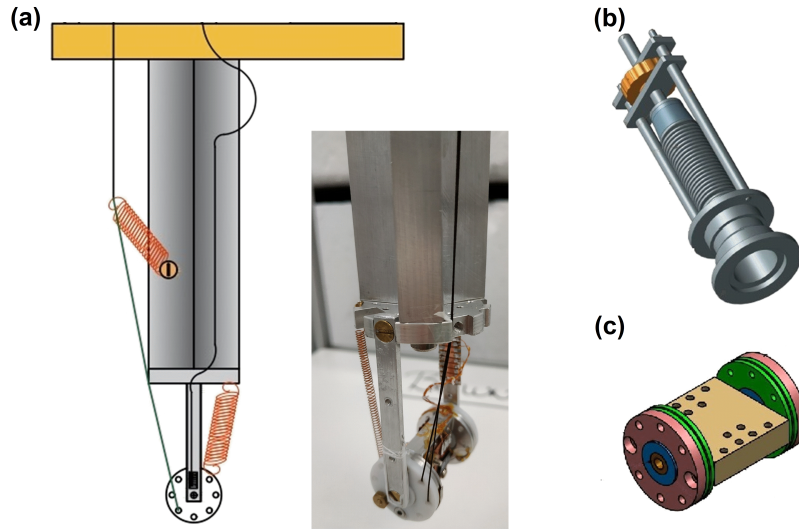


FIG. S4. (a) Scheme and photograph of the rotator. (b) Mechanical pulling systems at room temperature. (c) Detail of the rotator.

Available designs for rotators consist of gears operated through long tubes going to room temperature. Although the precision achieved with such rotators is very high, friction is often a problem and provides considerable heating at very low temperatures¹⁴. A solution is to use sapphire contacts with very low friction coefficients, although high rotation speeds still produce a sizeable power^{14,15}. An additional difficulty is that mechanical design has to consider carefully differential contraction of the whole set-up to avoid clamping at low temperatures. Piezo-driven systems have the advantage of providing compact designs on very small sizes and are commercially available^{16–18}. However, the application of high frequency signals to the piezoelectrics is nearly unavoidable, which also implies heating. Particularly for high speeds, heating can be a considerable problem, easily reaching the mW range. In addition, piezomotors rely on stick-slip motion, which is difficult to achieve at low temperatures. In another design used in some laboratories, a rotator is operated through Kevlar strings attached to a spring and a shaft that goes to room temperature¹⁹. This is similar to the wire based nanoscale sample positioning system described in Ref.20, which allows for precise cryogenic motion at low temperatures. Here we describe a rotating sample stage devoid of frictional heating. The rotator is operated by pulling on a string that goes to the top of the experiment (Fig. S4(a)), through a bellow at ambient temperature (Fig. S4(b)). The string is thermalized at each stage of the refrigerator and is maintained straight by using a spring connected to the support mechanism. At the level of the rotator, there is another spring connected to the support. It pulls the rotator back to the initial position when the tension in the string is released. The rotator is mounted with a copper cylinder as the rotation axis (Fig. S4(c)). The copper cylinder is firmly anchored at the end of the support. The pieces surrounding the cylinder are of teflon to allow for smooth rotation without generating heat. We have built rotators in Macor, Aluminum and plastic, details and drawings are provided in Ref.21.

To make the resistivity measurements, we use a four probe configuration and a conventional lock-in amplifier to measure the voltage. To apply the current, we use a Howland pump circuit²¹. We apply a voltage to the sample through a resistor R . The voltage is sensed at the exit of R by an operational amplifier and maintained constant, independently of the impedance of the sample, by a feedback driven through another operational amplifier. The current range can be modified by modifying R_x with a switch. The current range is given by the input voltage and the resistor R ^{22–24}. The impedance of the source increases as the inverse of the precision in the resistors used. Thus, the sensitivity to modifications in the current is considerably improved with respect to the use of a simple resistor in series and a voltage source. For instance, using 0.01% resistors implies source impedances multiplied by two orders of magnitude. The bandwidth of the circuit is limited by the operational amplifiers and a capacitor inserted parallel

to R and is in any case above 10kHz.

-
- ¹ W. Gao, X. Zhu, F. Zheng, M. Wu, J. Zhang, C. Xi, P. Zhang, Y. Zhang, N. Hao, W. Ning, and M. Tian, *A possible candidate for triply degenerate point fermions in trigonal layered PtBi₂*, [Nature Communications](#) **9**, 3249 (2018).
 - ² M. N. Ali, J. Xiong, S. Flynn, J. Tao, Q. D. Gibson, L. M. Schoop, T. Liang, N. Haldolaarachchige, M. Hirschberger, N. P. Ong, and R. J. Cava, *Large, non-saturating magnetoresistance in WTe₂*, [Nature](#) **514**, 205 EP (2014).
 - ³ F. F. Tafti, Q. D. Gibson, S. K. Kushwaha, N. Haldolaarachchige, and R. J. Cava, *Resistivity plateau and extreme magnetoresistance in LaSb*, [Nature Physics](#) **12**, 272 EP (2015).
 - ⁴ Y. L. Wang, L. R. Thoutam, Z. L. Xiao, J. Hu, S. Das, Z. Q. Mao, J. Wei, R. Divan, A. Luican-Mayer, G. W. Crabtree, and W. K. Kwok, *Origin of the turn-on temperature behavior in WTe₂*, [Phys. Rev. B](#) **92**, 180402 (2015).
 - ⁵ Y.-Y. Wang, Q.-H. Yu, P.-J. Guo, K. Liu, and T.-L. Xia, *Resistivity plateau and extremely large magnetoresistance in NbAs₂ and TaAs₂*, [Phys. Rev. B](#) **94**, 041103 (2016).
 - ⁶ W. Gao, N. Hao, F.-W. Zheng, W. Ning, M. Wu, X. Zhu, G. Zheng, J. Zhang, J. Lu, H. Zhang, C. Xi, J. Yang, H. Du, P. Zhang, Y. Zhang, and M. Tian, *Extremely large magnetoresistance in a topological semimetal candidate pyrite PtBi₂*, [Phys. Rev. Lett.](#) **118**, 256601 (2017).
 - ⁷ B. Chen, X. Duan, H. Wang, J. Du, Y. Zhou, C. Xu, Y. Zhang, L. Zhang, M. Wei, Z. Xia, C. Cao, J. Dai, M. Fang, and J. Yang, *Large magnetoresistance and superconductivity in α -gallium single crystals*, [npj Quantum Materials](#) **3**, 40 (2018).
 - ⁸ Z. Ren, A. A. Taskin, S. Sasaki, K. Segawa, and Y. Ando, *Large bulk resistivity and surface quantum oscillations in the topological insulator Bi₂Te₂Se*, [Phys. Rev. B](#) **82**, 241306 (2010).
 - ⁹ S. Gabáni, E. Bauer, S. Berger, K. Flachbart, Y. Paderno, C. Paul, V. Pavlík, and N. Shitsevalova, *Pressure-induced Fermi-liquid behavior in the Kondo insulator SmB₆: Possible transition through a quantum critical point*, [Phys. Rev. B](#) **67**, 172406 (2003).
 - ¹⁰ M. V. Kartsovnik, *High magnetic fields: A tool for studying electronic properties of layered organic metals*, [Chem. Rev.](#) **104**, 5737 (2004).
 - ¹¹ V. M. Yakovenko and B. K. Cooper, *Angular magnetoresistance oscillations in bilayers in tilted magnetic fields*, [Physica E: Low-dimensional Systems and Nanostructures](#) **34**, 128 (2006).
 - ¹² K. Yamaji, *On the angle dependence of the magnetoresistance in quasi-two-dimensional organic superconductors*, [Journal of the Physical Society of Japan](#) **58**, 1520 (1989).
 - ¹³ H. Weng, C. Fang, Z. Fang, and X. Dai, *Coexistence of Weyl fermion and massless triply degenerate nodal points*, [Phys. Rev. B](#) **94**, 165201 (2016).
 - ¹⁴ E. C. Palm and T. P. Murphy, *Very low friction rotator for use at low temperatures and high magnetic fields*, [Review of Scientific Instruments](#) **70**, 237 (1999).
 - ¹⁵ N. S. Selby, M. Crawford, L. Tracy, J. L. Reno, and W. Pan, *In situ biaxial rotation at low-temperatures in high magnetic fields*, [Review of Scientific Instruments](#) **85**, 095116 (2014).
 - ¹⁶ P. Wang, K. Huang, J. Sun, J. Hu, H. Fu, and X. Lin, *Piezo-driven sample rotation system with ultra-low electron temperature*, [Review of Scientific Instruments](#) **90**, 023905 (2019).
 - ¹⁷ L. A. Yeoh, A. Srinivasan, T. P. Martin, O. Kloch, A. P. Micolich, and A. R. Hamilton, *Piezoelectric rotator for studying quantum effects in semiconductor nanostructures at high magnetic fields and low temperatures*, [Review of Scientific Instruments](#) **81**, 113905 (2010).
 - ¹⁸ E. Ohmichi, S. Nagai, Y. Maeno, T. Ishiguro, H. Mizuno, and T. Nagamura, *Piezoelectrically driven rotator for use in high magnetic fields at low temperatures*, [Review of Scientific Instruments](#) **72**, 1914 (2001).
 - ¹⁹ S. T. Hannahs and E. C. Palm, *The national high magnetic field laboratory*, [Journal of Low Temperature Physics](#) **159**, 366 (2010).
 - ²⁰ H. Suderow, I. Guillaumon, and S. Vieira, *Compact very low temperature scanning tunneling microscope with mechanically driven horizontal linear positioning stage*, [Review of Scientific Instruments](#) **82**, 033711 (2011).
 - ²¹ *Drawings and circuit details are available at OSF.*
 - ²² *AN-1515 a comprehensive study of the Howland current pump, from Texas Instruments.*
 - ²³ J. Liu, X. Qiao, M. Wang, W. Zhang, G. Li, and L. Lin, *The differential howland current source with high signal to noise ratio for bioimpedance measurement system*, [Review of Scientific Instruments](#) **85**, 055111 (2014).
 - ²⁴ G. Hammond, C. Speake, and M. Stiff, *Noise analysis of a howland current source*, [International Journal of Electronics](#) **95** (2008).